NASA Contractor Report 189611
ICASE Report No. 92-6

ICASE

COMPRESSIBLE HOMOGENEOUS SHEAR: SIMULATION AND MODELING

S. Sarkar
G. Erlebacher
M. Y. Hussaini

Contract No. NAS1-18605
February 1992

Institute for Computer Applications in Science and Engineering
NASA Langley Research Center
Hampton, Virginia 23665-5225

Operated by the Universities Space Research Association

NASA
National Aeronautics and Space Administration
Langley Research Center
Hampton, Virginia 23665-5225

Compressible Homogeneous Shear: Simulation and Modeling*

S. Sarkar, G. Erlebacher, and M.Y. Hussaini
Institute for Computer Applications in Science and Engineering
NASA Langley Research Center
Hampton, VA 23665

ABSTRACT

The present study investigates compressibility effects on turbulence by direct numerical simulation of homogeneous shear flow. A primary observation is that the growth of the turbulent kinetic energy decreases with increasing turbulent Mach number. The sinks provided by compressible dissipation and the pressure-dilatation, along with reduced Reynolds shear stress, are shown to contribute to the reduced growth of kinetic energy. Models are proposed for these dilatational terms and verified by direct comparison with the simulations. The differences between the incompressible and compressible fields are brought out by the examination of spectra, statistical moments, and structure of the rate of strain tensor.

*Research was supported by the National Aeronautics and Space Administration under NASA Contract No. NAS1-18605 while the authors were in residence at the Institute for Computer Applications in Science and Engineering (ICASE), NASA Langley Research Center, Hampton, VA 23665.

1 Introduction

Homogeneous turbulent flow has long been viewed as a simple model of turbulence which is sufficiently realistic to have fundamental physical features that persist in more complex flows. For example, hairpin vortices which have been observed in boundary layer experiments and simulations of channel flow, have been identified through direct numerical simulation (DNS) of homogeneous shear flow by Rogers and Moin (1987). Similarly, the longitudinal streaks observed in wall boundary layers have been shown by the simulations of Lee, Kim and Moin (1990) to exist in homogeneous shear flow when the shear rate is high enough to be comparable to those encountered near the wall in boundary layers. Rogallo (1981), who was the first to perform DNS of this flow, showed by direct comparison with physical experiments that the simulated flow statistics were in good agreement with experimental data.

In the past several years, there has been a strong activity in the area of compressible turbulent simulations. The first fundamental study of compressible isotropic turbulence was conducted by Passot and Pouquet (1987) who demonstrated the presence of shocks in the flow. Their results motivated the study by Erlebacher et al. (1990) to classify the different possible regimes in isotropic turbulence attainable from arbitrary initial conditions. They quantified the conditions for the presence or absence of shocks. Other results on decaying isotropic turbulence can be found in Sarkar et al. (1989), Lee, Lele and Moin (1990), and Zang, Dahlburg, and Dahlburg (1992). Results on forced isotropic turbulence are also available (Kida and Orszag 1990). Simulations have now moved on to the next level of complexity, namely, homogeneous turbulence subjected to a linear mean velocity field. For example, Coleman and Mansour (1991) have considered turbulence subjected to homogeneous compression.

Homogeneous shear turbulence has a production term which continuously feeds energy into the system, which then cascades down to the smaller scales. This flow exhibits some of the properties of incompressible turbulent shear flows, with the added presence of acoustic waves, density fluctuations, and dilatational velocity fields. Direct numerical simulations of such flows can provide complete statistics not available from physical experiments. Compressibility effects on the flow can be obtained from the simulations, and perhaps more importantly, mechanisms responsible for these effects can be identified, and turbulence models for compressibility-related phenomena can be devised. The compressible problem was considered by Feiereisen et al. (1982) who performed relatively low resolution 64^3 simulations and concluded that compressibility effects are small. Recently Blaisdell, Mansour and Reynolds (1990) have also considered compressible shear flow, and identified eddy shocklets

in the flow for high enough turbulence Reynolds and Mach number.

Research on the small-scale properties of homogeneous turbulence is primarily focussed on understanding the intermittency of high dissipation regions. It has been numerically established that the rate of strain tensor has a preferred shape in regions of strong dissipation (Ashurst et al. 1987b). Furthermore, the vorticity tends to align with the intermediate eigenvalue (whose most probable sign is positive). While this alignment property of the vorticity is a consequence of a simplification of the Euler equations (Vieillefosse 1984), the shape of the tensor is still unexplained. Alignment of other vectors have been considered by Ashurst et al. (1987a).

In this paper, we use databases from the DNS of homogeneous compressible turbulence to clarify the sources of reduced growth of kinetic energy with increased levels of compressibility. This is then used to propose a new decomposition of pressure into incompressible and compressible components. In turn, this leads to an improved model for the pressure-dilatation term. Finally, we analyze the rate of strain tensor after decomposition into solenoidal and irrotational components. Differences between the two tensors are brought out through the use of one-dimensional probability functions.

2 Governing Equations

The compressible Navier-Stokes equations are written in a frame of reference moving with the mean flow $\overline{u}_1$. This transformation, which was introduced by Rogallo (1981) for incompressible homogeneous shear, removes the explicit dependence on $\overline{u}_1(x_2)$ in the exact equations for the fluctuating velocity, thus allowing periodic boundary conditions in the x_2 direction. The relation between the moving frame x_i^* and the lab frame x_i is

$$x_1^* = x_1 - Stx_2 \quad , \quad x_2^* = x_2 \quad , \quad x_3^* = x_3$$

Here S denotes the constant shear rate $\bar{u}_{1,2}$. In the transformed frame x_i^*, the compressible Navier-Stokes equations take the form

$$\partial_t \rho + (\rho u_i')_{,i} - St(\rho u_2')_{,1} = 0 \tag{1}$$

$$\begin{aligned} \partial_t(\rho u_i') + (\rho u_j' u_i')_{,j} &= -p_{,i} + \tau'_{ij,j} - S\rho u_2'\delta_{i1} \\ &+ St(\rho u_2' u_i')_{,1} + Stp_{,1}\delta_{i2} - St\tau'_{i2,1} \end{aligned} \tag{2}$$

$$\begin{aligned} \partial_t p + u_j' p_{,j} + \gamma p u'_{j,j} &= Stu_2' p_{,1} + \gamma Stpu'_{2,1} + \Phi \\ &+ (\gamma - 1)\kappa[T_{,jj} - 2StT_{,12} + S^2t^2T_{,11}] \end{aligned} \tag{3}$$

$$p = \rho RT \tag{4}$$

where $\Phi = \tau_{ij}\partial u_i/\partial x_j$ is the dissipation function, τ_{ij} the viscous stress, u_i' the fluctuating velocity, ρ the instantaneous density, p the pressure, T the temperature, R the gas constant. The molecular viscosity μ, and thermal conductivity κ are taken to be constant. In terms like $u'_{i,j}$ in the above system, the comma denotes a derivative with respect to the transformed coordinates x_i^*.

A Fourier collocation method is used for the spatial discretization of the governing equations. A third order, low storage Runge-Kutta scheme is used for advancing the solution in time. The nonlinear terms are dealiased by discarding modes lying in the highest third of the wave number range resolved by the grid. This procedure fully dealiases the quadratic and not the cubic non-linearities in the Navier-Stokes equations.

3 Statistical Moments and Spectra

We have performed simulations for a variety of initial conditions and obtained turbulent fields with Taylor microscale Reynolds numbers Re_λ up to 45 and turbulent Mach numbers M_t up to 0.7. Note that $Re_\lambda = q\lambda/\nu$ where $q = \sqrt{\overline{u_i'u_i'}}$ and $\lambda = q/\sqrt{\overline{\omega_i'\omega_i'}}$, while $M_t = q/\bar{c}$ where $\bar{c}$ is the mean speed of sound. All the simulations have been performed with $\gamma = 1.4$, and Prandtl number $Pr = 0.7$. The computational domain is a cube with side 2π. The results discussed here were obtained with a uniform 128^3 mesh overlaying the computational domain.

In the case of homogeneous shear flow, the mean velocity $\bar{u}_i$ varies linearly in space and remains invariant in time. The mean density $\overline{\rho}$ is uniform initially and does not evolve in time. However, due to the mean viscous dissipation, the mean pressure $\overline{p}$ and temperature $\overline{T}$ increase in time.

3.1 Effect of Compressibility on Kinetic Energy

Figs. 2-5 show results from two selected cases which have identical initial data for the velocity and thermodynamic variables. The initial data is incompressible, that is, the density is constant and the divergence $\nabla.\mathbf{u} = 0$. The initial pressure is calculated from the Poisson equation appropriate for incompressible flows, and the temperature is obtained from the ideal gas equation of state. The variable parameters for the problem are the shear rate S, viscosity μ, and the speed of sound $\bar{c}$. The two cases have identical values for S and μ, but different values for the speed of sound $\bar{c}$ leading to different initial Mach numbers $M_{t,0}$. Table 1 lists the initial parameters for these cases. The simulation of Case 1 ran up to $St = 18$

when $M_t = 0.46$ and $Re_\lambda = 43$, while Case 2 was continued up to $St = 21$ when $M_t = 0.67$ and $Re_\lambda = 41$.

The Favre-averaged kinetic energy K is defined by $K = \widetilde{\rho u_i'' u_i''}/2\overline{\rho}$. Note that the overbar over a variable denotes a conventional Reynolds average, while the overtilde denotes a Favre average. A single superscript $'$ represents fluctuations with respect to the Reynolds average, while a double superscript $''$ signifies fluctuations with respect to the Favre average. The evolution of the kinetic energy K as a function of non-dimensional time St is shown in Fig. 1. Physical experiments and DNS of the incompressible case indicate that K, after an initial transient, evolves as $K_0 \exp(\Lambda St)$. The feature of exponential growth is carried over to the compressible case, as evidenced by the approximately linear regime in the plot of $\ln(K/K_0)$ in Fig. 2 for $St > 7$. Although the picture of exponential growth survives, the growth rate of K shows a significant decline with a decrease in the speed of sound. Figure 3 shows that the growth rate $\Lambda = d(\ln K/K_0)/d(St)$ decreases by about 30% when M_t increases from 0.2 to 0.4. We note that the reduction of kinetic energy growth rate with increasing compressibility is a consistent trend in all our simulations.

In order to understand the phenomenon of reduced growth rate of kinetic energy, we consider the equation governing the kinetic energy of turbulence in homogeneous shear which is

$$\frac{d}{dt}(\overline{\rho}K) = \overline{p}\mathcal{P} - \overline{\rho}\epsilon_s - \overline{\rho}\epsilon_c + \overline{p'd'} \tag{5}$$

where $\mathcal{P} = -S\widetilde{u_1'' u_2''}$ is the production, $\epsilon_s = \overline{\nu\omega_i'\omega_i'}$ the solenoidal dissipation rate, $\epsilon_c = (4/3)\overline{\nu d'^2}$ the compressible dissipation rate and $\overline{p'd'}$ the pressure-dilatation. The last two terms represent the explicit influence of the non-solenoidal nature of the fluctuating velocity field in the kinetic energy budget.

If the notion of exponential growth in homogeneous shear flow is correct, Λ should asymptote to a constant. The relative importance of the various terms on the rhs of (5) can be gauged by their contribution to Λ. We, therefore, normalize (5) by $\overline{\rho}SK$. The terms on the rhs of (5) are plotted in Fig. 4 after being thus normalized. According to Figs. 4a-4b,the dilatational terms are negative and reduce Λ. By $St = 20$, the combined contribution of the dilatational terms is approximately 20% of Λ, implying that they need to be considered in turbulence modeling. The normalized production, $\mathcal{P}/SK$, is plotted in Fig. 4c. The normalized production in Case 2 begins to deviate from that in Case 1 around $St = 5$, and eventually asymptotes to a value noticeably smaller than in Case 1. Thus, the production is reduced due to compressibility. The normalized dissipation in Fig. 4d also shows a decrease in Case 2 relative to Case 1, but to a smaller degree than the production. The reduction in growth rate of K in Case 2 relative to Case 1 seems to be primarily due to the dilatational terms during the early phase of the evolution and, for the later phase ($St > 8$), is related to

a decreased level of production.

3.2 Measures of Compressibility

Apart from the differences in the evolution of turbulence statistics in the case of compressible flow relative to incompressible flow, a question that arises is how compressible is the turbulence? The turbulent Mach number $M_t = \sqrt{2K}/\bar{c}$ and the normalized rms density $\rho_{\rm rms}/\bar{\rho}$ are measures of departure from incompressibility, since both these quantities are zero for strictly incompressible flow. M_t shows a monotone increase in Fig. 5a reaching a maximum of 0.6, which is larger than the upper bound of M_t in free shear layers and wall boundary layers encountered in aerodynamic practice. Figure 5b shows that, after starting from zero density fluctuations, both simulations develop significant rms density levels at $St = 18$, and most of the increase in rms density occurs rapidly within $St < 3$ for Case 2 (with the higher initial M_t). The velocity field is no longer solenoidal in compressible flow, that is, $d = \nabla \cdot \mathbf{u} \neq 0$. For homogeneous flow, the Helmholtz decomposition gives a unique decomposition of the velocity field into incompressible and compressible components by $\mathbf{u} = \mathbf{u}^I + \mathbf{u}^C$, where $\nabla \cdot \mathbf{u}^I = 0$ and $\nabla \times \mathbf{u}^C = 0$. The departure of the velocity field from solenoidality is another measure of compressibility, and can be represented by the ratio of dilatational variance to enstrophy $\chi_d = \overline{d'^2}/\overline{\omega_i'\omega_i'}$ or by the fraction of kinetic energy which is dilatational $\chi_K = K_C/K$. The former quantity χ_d is more general, because the Helmholtz decomposition required for obtaining K_C is unique only for homogeneous flows. Figure 6 shows that after an initial transient, χ_d increases monotonically for Case 1, but levels off at about 8% for Case 2. The quantity χ_K (not plotted here) is comparable to χ_d, leveling off at approximately 6% for Case 2. Since the mean shear leads to anisotropy of the Reynolds stress tensor, the dilatational fraction of each Reynolds stress component is obtained. Except for the transverse component $\overline{u_2'u_2'}$, the dilatational contribution to the Reynolds stress tensor was a few percent, comparable to the magnitude of χ_K. The ratio of $\overline{u_2^{C'}u_2^{C'}}/\overline{u_2'u_2'}$ is substantially larger, as shown in Fig. 7. Since the dilatational component is a relatively poor mixer of scalar compared to the vortical component, the large ratio of $\overline{u_2^{C'}u_2^{C'}}/\overline{u_2'u_2'}$ implies that mixing is preferentially decreased by compressibility in the direction of shear.

3.3 Compressible and Solenoidal Spectra

The Fourier component of the velocity is decomposed into components perpendicular and parallel to the wave number vector from which the solenoidal spectrum $E_s(k)$ and compressible spectrum $E_c(k)$ are calculated. Figure 8 compares the solenoidal and compressible spectra at St=15 (when $M_t = 0.55$) for Case 2. The compressible energy is small relative to

the incompressible energy for all modes. The compressible spectrum is flatter at low wave numbers ($k < 16$) relative to the incompressible spectrum. The two spectra have similar slopes in the intermediate wave number range. The solenoidal spectrum is compared in Fig. 9 between an incompressible run ($M_t = 0$) and a compressible run at $St = 17$. The compressible run has an initial M_t of 0.4 and the initial velocity and pressure fields are the same as in the incompressible run. ¿From Fig. 9, it appears that the shape of the solenoidal spectrum is not altered by compressibility, even though the compressible fluctuations are non-negligible at this time- $\rho_{\rm rms}/\overline{\rho} = 0.12$ and $\chi_k = K_c/K = 0.05$. However, the pressure spectrum in Fig. 10 shows significant differences between these two cases. In the compressible case, the pressure spectrum seems to be relatively flatter than in the incompressible case.

4 Modeling the Dilatational Terms

We showed in Fig. 4 that the compressible dissipation ϵ_c and the pressure-dilatation $\overline{p'd'}$ contribute significantly to the kinetic energy budget and therefore require modeling. In Sarkar et al. (1991), we proposed a model for the compressible dissipation $\epsilon_c = \alpha_1 \epsilon_s M_t^2$ based on an asymptotic analysis and DNS of isotropic turbulence. In the present simulations, after starting from a variety of initial conditions, $\epsilon_c \simeq 0.5\epsilon_s M_t^2$, suggesting that $\alpha_1 = 0.5$.

Our direct numerical simulations of isotropic turbulence and homogeneous shear flow provided a data base for the pressure-dilatation and suggested a theoretical approach towards modeling it. The evolution of the pressure-dilatation $\overline{p'd'}$ for Case 1 is depicted by the solid curve in Fig. 11. ¿From numerical experiments, it was found that the nominal time period of the oscillations in $\overline{p'd'}$ decreased approximately linearly with the speed of sound. This suggested that one could isolate the oscillatory part of $\overline{p'd'}$ by decomposing the fluctuating pressure p' into the sum of an incompressible part $p^{I'}$ and a compressible part $p^{C'}$. The incompressible pressure $p^{I'}$ satisfies

$$\nabla^2 p^{I'} = -2\tilde{u}_{i,j}\overline{\rho}u'_{j,i} - 2\tilde{u}_{i,i}\overline{\rho}u'_{j,j} - \overline{\rho}(u_i'u_j')_{,ij} - 2\overline{u}_{i,ij}(\overline{\rho}u_j') \qquad (6)$$

while the remainder $p^{C'}$ is the compressible pressure. The rhs of (6) collects all terms that depend on $\overline{\rho}$ in the equation obtained by taking the divergence of the momentum equation. In the simulations, since p' is available from the compressible Navier-Stokes solution and $p^{I'}$ is evaluated from (6), we obtain $p^{C'}$ as the difference $p' - p^{I'}$. Since $p' = p^{I'} + p^{C'}$ we have $\overline{p'd'} = \overline{p^{I'}d'} + \overline{p^{C'}d'}$. The oscillations are substantial only for $\overline{p^{C'}d'}$ (dotted curve in Fig. 11), and furthermore, the peaks and valleys in the evolution of $\overline{p^{C'}d'}$ seem to be much more symmetric around the origin than those in $\overline{p'd'}$ (solid curve in Fig. 11). The component $\overline{p^{I'}d'}$ (dash-dotted curve in Fig. 11) does not have strong temporal oscillations, and shows

a systematic decrease with time. In order to gauge the relative importance of the two components $\overline{p^{C'}d'}$ and $\overline{p^{I'}d'}$ of the pressure-dilatation in the evolution of the turbulent kinetic energy, we calculate the time integrals of these components. The integrated contribution of $\overline{p^{I'}d'}$ is about an order of magnitude larger than that of $\overline{p^{C'}d'}$ in Case 2. Examination of other DNS cases indicates that, in general, $\overline{p^{C'}d'}$ has a negligible contribution to the turbulent kinetic energy evolution relative to $\overline{p^{I'}d'}$. Therefore, it seems that only the component $\overline{p^{I'}d'}$ of the pressure-dilatation requires modeling in shear flows.

In order to model $\overline{p^{I'}d'}$, we consider the Poisson equation (6) for the incompressible pressure. After splitting the pressure into a rapid part $p^{R'}$ and a slow part $p^{S'}$, we obtain the following exact expressions for the rapid pressure-dilatation and slow pressure-dilatation:

$$\overline{p^{R'}d'} = 2\overline{\rho}\tilde{u}_{m,n}\int \frac{k_m k_j}{k^2} E_{nj}\,d\mathrm{k} \tag{7}$$

$$\overline{p^{S'}d'} = \overline{\rho}\int \frac{k_m k_l k_j}{k^2}(i\widehat{u_l u_j}\hat{u}_m^* - i\widehat{u_l u_j}^*\hat{u}_m)\,d\mathrm{k} \tag{8}$$

Here $\hat{\phi}^*$ denotes the complex conjugate of the Fourier transform $\hat{\phi}$ and E_{nj} represents the spectrum of the Reynolds stress tensor $\overline{u_n' u_j'}$. Using scaling arguments (see Sarkar (1991) for details) to simplify (7)-(8) we find that $\overline{p^{R'}d'}$ depends on the production $\mathcal{P}$ while $\overline{p^{S'}d'}$ depends on the dissipation ϵ_s. Finally, we propose the following model for the pressure-dilatation:

$$\overline{p'd'} = \alpha_2\overline{\rho}\tilde{u}_{i,j}b_{ij}q^2 M_t + \alpha_3\overline{\rho}\epsilon_s M_t^2 + \frac{8}{3}\overline{\rho}\tilde{u}_{i,i}\chi(M_t)q^2 \tag{9}$$

where $b_{ij} = \widetilde{u_i'' u_j''}/q^2 - \delta_{ij}/3$ is the anisotropy tensor, $M_t = \sqrt{2K}/\overline{c}$ the turbulent Mach number, and ϵ_s the solenoidal dissipation. To obtain the functional dependence $\chi(M_t)$ in the last term of Eq. (9), one would require data from a flow with mean homogeneous compression. In this paper, we validate and calibrate the first two terms in the model for $\overline{p'd'}$. In homogeneous shear, the model becomes

$$\overline{p'd'} = -\alpha_2\overline{\rho}\mathcal{P}M_t + \alpha_3\overline{\rho}\epsilon_s M_t^2 \tag{10}$$

where $\mathcal{P} = -S\widetilde{u_1'' u_2''}$. Because the production $\mathcal{P} = 0$ in decaying isotropic turbulence, the variation of the incompressible pressure-dilatation with ϵ_s can be verified using DNS of isotropic turbulence. The ratio $\overline{p^{I'}d'}/(\overline{\rho}\epsilon_s M_t^2)$ is shown as a function of non-dimensional time in Fig. 12. The decaying isotropic turbulence simulations, D1,D2 and D3 start with $M_{t,0}$ of 0.6,0.5, and 0.4 respectively. $\overline{p^{I'}d'}/(\overline{\rho}\epsilon_s M_t^2)$ reaches an equilibrium value by a time of 0.25, substantiating the validity of the second term in (9). Based on the DNS value of the equilibrium ratio, the model coefficient α_3 in (9) is taken to be 0.2. The remaining part of the model for the pressure-dilatation is calibrated against simulations of homogeneous

shear flow. Fig. 13 shows results from three cases S1,S2 and S3 with $M_{t,0}$ of 0.2,0.3, and 0.4 respectively. Cases S2 and S3 have shear S=15, while Case S1 has S=20. After $St = 5$, the ratio $(\overline{p^{I'}d'} - 0.2\overline{\rho}\epsilon_s M_t^2)/(\overline{\rho}\mathcal{P}M_t)$ evolves in a similar fashion for the three cases and exhibits a slight decrease with time. In the period $5 < St < 15$, the three cases S1-S3 encompass a range of turbulent Mach numbers of $0.21 < M_t < 0.65$. The results of Fig. 13 suggest that, with a coefficient $\alpha_2 = 0.15$, the proposed model (9) is able to parametrize the pressure-dilatation for $0.2 < M_t < 0.6$.

5 Structure of the Rate of Strain Tensor

In this section, we study several properties of the rate of strain tensor S_{ij} to help identify characteristics of the flow which are solely the result of compressibility effects, and how these characteristics differ from corresponding properties in an incompressible turbulent flow. Because the flow is anisotropic, it is useful to consider characteristics of the flow both with respect to the laboratory frame of reference, and with respect to a frame of reference attached to, and rotating with an individual fluid element. Global orientation properties of S_{ij} are established by studying the principal directions of S_{ij} in the laboratory frame of reference. (In isotropic turbulence, this diagnostic does not provide useful information.) On the other hand, local properties can be characterized by considering the relative orientation of vectors such as velocity, vorticity or scalar gradients, with respect to the principal directions of S_{ij}.

We consider the rate of strain tensor, decomposed according to

$$S_{ij} = S_{ij}^C + S_{ij}^I + \frac{1}{3} u_{i,i} \delta_{ij} \tag{11}$$

where S_{ij}^I and S_{ij}^C are respectively constructed from the solenoidal and compressible (irrotational) velocities $\mathbf{u}^I$ and $\mathbf{u}^C$. Both S_{ij}^I and S_{ij}^C are deviatoric. The properties of these tensors are expressed in terms of invariant quantities, i.e. eigenvalues and eigenvectors. Because S_{ij} is symmetric, its eigenvalues λ_i, $i = 1,2,3$ are real, and its eigenvectors are in the directions of maximal or minimal extension (depending on the sign of the λ_i) of the tensor. These directions are given by the tensor's three eigenvectors. For future reference, the eigenvalues are ordered from smallest to largest:

$$\lambda_1 \leq \lambda_2 \leq \lambda_3. \tag{12}$$

The first three invariants of the tensor S_{ij}, defined as the coefficients of the polynomial characteristic equation, are related to small scale phenomena, and can be expressed in terms of the eigenvalues. These relationships are:

$$I = -(\lambda_1 + \lambda_2 + \lambda_3)$$

$$II = \lambda_1\lambda_2 + \lambda_1\lambda_3 + \lambda_2\lambda_3$$
$$III = -\lambda_1\lambda_2\lambda_3$$

If the tensor is deviatoric, $I = 0$, $-II = S_{ij}S_{ji}$ which for incompressible flow is proportional to the dissipation, and in isotropic flow, III is proportional to the third moment of the velocity gradient probability distribution function (pdf).

We present results from one simulation with $S = 15$, and $\mu = 1/150$, $M_{t0} = 0.3$, $R_{\lambda 0} = 20$ and incompressible initial data. The simulated flow is analyzed at $St = 1, 3, 5, 7, 9$, which are all sufficiently resolved. More details of this analysis can be found in Erlebacher, Sarkar and Hussaini (1991). Note that all the pdf's that follow are unconditioned and unweighted. Sampling for the pdf's (probability density function) is done on a grid resolution of $48\times96\times96$ although the simulation was performed on a 96^3 mesh. This provides over 400,000 sample points.

The pdf of λ_2^I/λ_1^I and λ_2^C/λ_1^C are shown in Figs. 14 and 15. Both plots show that after an initial transient, the eigenvalue ratios have single peaks. These are located at -0.25 for the solenoidal ratio, and at approximately -0.375 for the irrotational ratio. As a consequence, the rate of strain tensors S_{ij}^I and S_{ij}^C, respectively, have preferred strains in the ratios $(-4 : 1 : 3)$ and $(-8 : 3 : 5)$ along the principal axes. Conditioning of λ_2^I/λ_1^I with respect to ϵ_s sharpens the peak for higher values of dissipation. Further processing of the irrotational ratio distribution is underway. A check of the pdf of the irrotational ratio was also performed from a 128^3 database (Case 2) with 800,000 sample points, and its shape is qualitatively similar with the peak at -0.375. Note that the pdf of the irrotational ratio is more broadband than that of the solenoidal ratio. However, the location of the peak is well defined, and constant in time. This equilibrium structure of $(-4 : 1 : 3)$ for S_{ij} is observed in incompressible flow, first by Ashurst, Kerstein, Kerr & Gibson (1987). They considered the statistics of $(\lambda_2^I)^2/(S_{ij}^I S_{ij}^I)$ conditioned on the dissipation and found that the preferred ratio was most dominant in regions of high dissipation. In a later work, Chen et al. (1990) displayed scattergrams of II versus III based on incompressible mixing layer DNS data, which clearly demonstrated that III is proportional to $(-II)^{3/2}$ in the regions of highest dissipation. This is in fact a statement about the preferred shape of the S_{ij}^I principal ellipsoid. Our results indicate that compressibility does not substantially affect this preferred structure of the solenoidal S_{ij}^I.

The distribution of λ_1^I and λ_1^C show some distinctive differences, as illustrated in Figs. 16-17. Both figures show negative skewness of the distributions, and a flattening in time, although the effect is much more severe for λ_1^C. On both plots, the most probable value for the eigenvalue shifts towards more negative values. In the irrotational case, the effect is extremely strong. However, the most probable ratio of λ_2^C to λ_1^C (see Fig. 15) remains

invariant in time. Figure 17 also indicates that the amount of change in the distribution of λ_1^C decreases with time, but there is no strong evidence that the shape of the pdf is evolving towards a steady state.

Information on structural differences in the flow as they relate to preferred directions of straining for both the solenoidal and dilatational components of the flow are presented next. After the eigenvectors of the rate of strain tensors are normalized to unity, we compute the angle θ_{ij} between eigenvector $\mathbf{f}_i$ and the unit vector in the coordinate direction x_j. The pdf's of $|\cos\theta_{ij}^I|$ and $|\cos\theta_{ij}^C|$ are then computed. The cosine of θ is chosen instead of θ so that the probability density function based on a Gaussian distribution for the velocity derivatives is flat. In Figs. 18-19, we respectively plot the pdf of $|\cos\theta_{1i}^I|$ and $|\cos\theta_{1i}^C|$, $(i = 1,2,3)$ at $St = 9$ to illustrate that the solenoidal and irrotational rate of strain tensors have different preferential alignments in the laboratory frame of reference. Note that $R_\lambda = 33$ at this time. The direction of maximum compression of S_{ij}^I ($\mathbf{f}_1^I$) tends to be at approximately 45° to both the x and y axes, with no preferred orientation with respect to z. The alignment of $\mathbf{f}_3^I$ is also in the 45° direction, while $\mathbf{f}_2^I$ has no unambiguous preferred direction. The irrotational rate of strain tensor exhibits markedly different properties. Most of the distributions of $\cos\theta_{ij}$ have two strong peaks, thus indicating two preferred directions of alignment. For example, $\mathbf{f}_1^C$ is most often aligned along one of the three coordinate axes. This is true of the other two principal directions, but to a lesser degree. Interestingly enough, all three pdf's of $\mathbf{f}_i^C$ exhibit a valley in the neighborhood of 45°. Statistics based on the database of Case 2 (at a higher shear and higher Reynolds number than the results plotted in the preceding figures) show that the pdf's of $|\cos\theta_{1i}^I|$ and $|\cos\theta_{1i}^C|$ are sharper. In particular, the tendency for $\mathbf{f}_1^I$ to align is strongest in a direction at 30° to the x axis and not 45°. Finally, we notice that all the pdf's of $|\cos\theta_{ij}|$ tend towards a steady distribution with increasing St. The distribution of $|\cos\theta_{ij}^C|$ reaches an equilibriated state at a much earlier stage than does $|\cos\theta_{ij}^I|$.

6 Conclusions

We have performed DNS of homogeneous shear using a 128^3 grid to ascertain the influence of compressibility on turbulence statistics and structure. The primary result is the stabilizing effect of compressibility on the growth of kinetic energy. We find that the reduction in growth rate is due to the pressure-dilatation and compressible dissipation acting as sinks for the kinetic energy, and due to the reduced level of the Reynolds shear stress. After starting with zero density fluctuations, the simulations develop significant density fluctuations and moderate levels of energy in the dilatational component. The dilatational velocity component is strongly anisotropic, and consequently its contribution to the transverse rms velocity is

much larger than to the other rms turbulent velocities. Although, the turbulent Mach number and rms density fluctuations are significantly large, the shape of the energy spectrum is practically unaffected by compressibility. However, the pressure spectrum is much flatter for the compressible case relative to the incompressible case. The eigenvalues and eigenvectors of both the solenoidal and irrotational rate of strain tensors were examined for preferred structure. In principal axes, the solenoidal rate of strain tensor has a preferred shape of (-4:1:3) in accord with previous results available for incompressible flow. The irrotational rate of strain tensor has a different preferred shape. The pressure-dilatation correlation needs to be modeled for compressible flow. We consider a form of the pressure equation obtained by taking the divergence of the momentum equation, deduce a formal solution for the pressure-dilatation, and then simplify to obtain a model for the pressure-dilatation. The model seems to compare well with DNS data in isotropic turbulence and homogeneous shear turbulence.

References

[1] Ashurst, Wm. T., Chen, J.-Y.,and Rogers, M.M.: Pressure Gradient Alignment with Strain Rate and Scalar Gradient in Simulated Navier-Stokes Turbulence.*Phys. Fluids A*, **30**, (1987a) 3293-3294.

[2] Ashurst, Wm. T., Kerstein, A.R., Kerr, R.M., and Gibson, C.H.: Alignment of Vorticity and Scalar Gradient with Strain Rate in Simulated Navier-Stokes Turbulence. Phys. Fluids **30**, (1987b) 2343-2353.

[3] Blaisdell, G.A., Mansour, N.N, and Reynolds, W.C.: Numerical simulation of Compressible Homogeneous Turbulence, *Stanford University Report No. TF-50* (1991).

[4] Chen, J.H., Chong, M.S., Soria, J., Sondergaard, R., Perry, A.E., Rogers, M., Moser, R., and Cantwell, B.J.: A study of the topology of dissipating motions in direct numerical simulations of time-developing compressible and incompressible mixing layers.*CTR, Proceedings of Summer Program* (1990).

[5] Coleman, G.N., and Mansour, N.N.: Modeling the rapid spherical compression of isotropic turbulence. *Phys. Fluids A*,**3** (1991) 2255-2259.

[6] Erlebacher, G., Hussaini, M.Y., Kreiss, H.O., and Sarkar, S.: The Analysis and Simulation of Compressible Turbulence. *Theoret. Comput. Fluid Dynamics*, **2** (1990) 73-95.

[7] Erlebacher, G., Sarkar, S., Hussaini, M. Y.: Structure of Compressible Turbulence in Homogeneous Shear Flow. *ICASE Report* (in preparation).

[8] Feiereisen, W.J., Shirani, E., Ferziger, J.H., and Reynolds, W.C.: Direct Simulation of Homogeneous Turbulent Shear Flows on the Illiac IV Computer. In *Turbulent Shear Flows 3* (1982) 309-319. Springer-Verlag, Berlin.

[9] Kida, S. and Oszag, S.A.: Energy and Spectral Dynamics in Forced Compressible Turbulence. *J. Sci. Comp.*, **5**, (1990) 85.

[10] Lee, M.J., Kim, and J., Moin, P.: Structure of turbulence at high shear rate. *J. Fluid Mech.*, **216**, (1990) 561-583.

[11] Lee, S., Lele, S.K., and Moin, P.: Eddy-shocklets in Decaying Compressible Turbulence. *CTR Manuscript 117* (1990).

[12] Passot, T.: Simulations numeriques d'ecoulements compressibles homogenes en regime turbulent : application aux nuages moleculaires. *Ph. D. Thesis, University of Paris* (1987).

[13] Rogallo, R.S.: Numerical Experiments in Homogeneous Turbulence. *NASA TM 81315* (1981).

[14] Rogers, M.M., and Moin, P.: The Structure of the Vorticity Field in Homogeneous Turbulent Flows. *J. Fluid Mech.*, **176** (1987) 33-66.

[15] Sarkar, S., Erlebacher, G., Hussaini, M.Y., and Kreiss, H.O.: The Analysis and Modeling of Dilatational Terms in Compressible Turbulence. *J. Fluid Mech*, **227** (1989) 473-493.

[16] Sarkar, S., Erlebacher, G., and Hussaini, M.Y.: Direct Simulation of Compressible Turbulence in a Shear Flow. *Theor. Comput. Fluid Dyn.*, **2** (1991) 291-305.

[17] Sarkar, S.: Modeling the Pressure-dilatation Correlation. *ICASE Report 91-42* (1991).

[18] Vieillefosse, P.: Internal Motion of a Small Element of Fluid in an Inviscid Flow. Physica **125 A**,(1984) 150-162.

[19] Zang, T.A., Dahlburg, R.B., and Dahlburg, J.P.: Direct and Large-eddy Simulations of Compressible, Isotropic, Navier-Stokes Turbulence. *Phys. Fluids A* (in press).

Case	S	ν	$M_{t,0}$	$R_{\lambda,0}$	ρ'	d'
1	20	1/150	0.2	14	0	0
2	20	1/150	0.4	14	0	0

Table 1: Parameters for the DNS cases of homogeneous shear flow

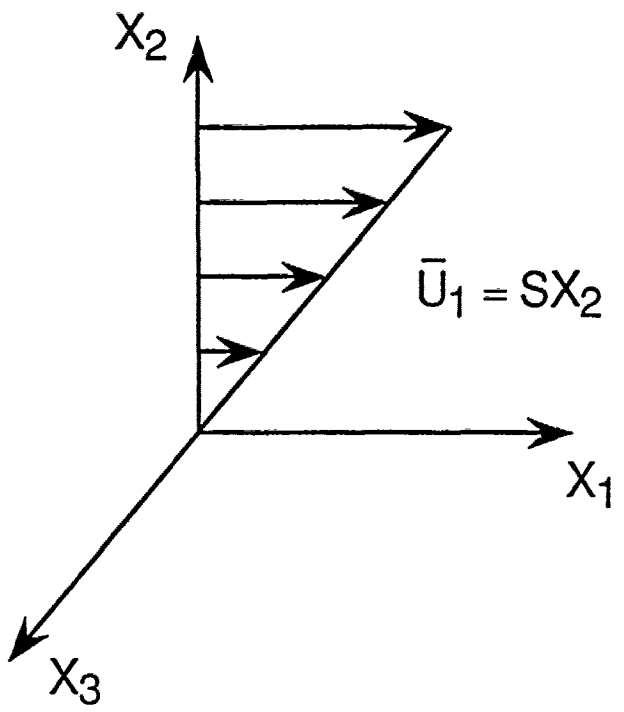

Fig. 1. Schematic of homogeneous shear flow.

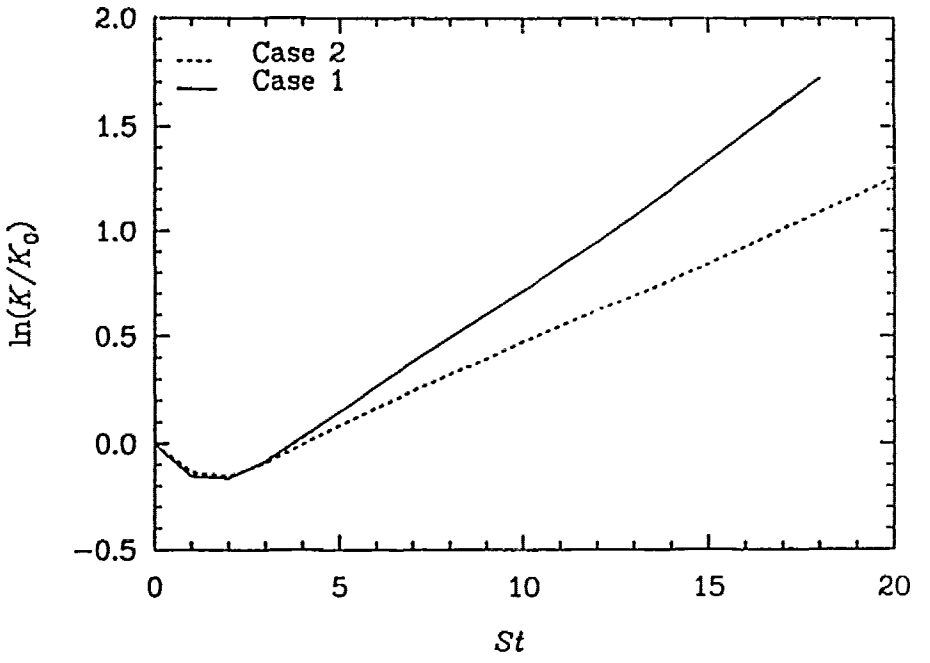

Fig. 2. Time evolution of turbulent kinetic energy.

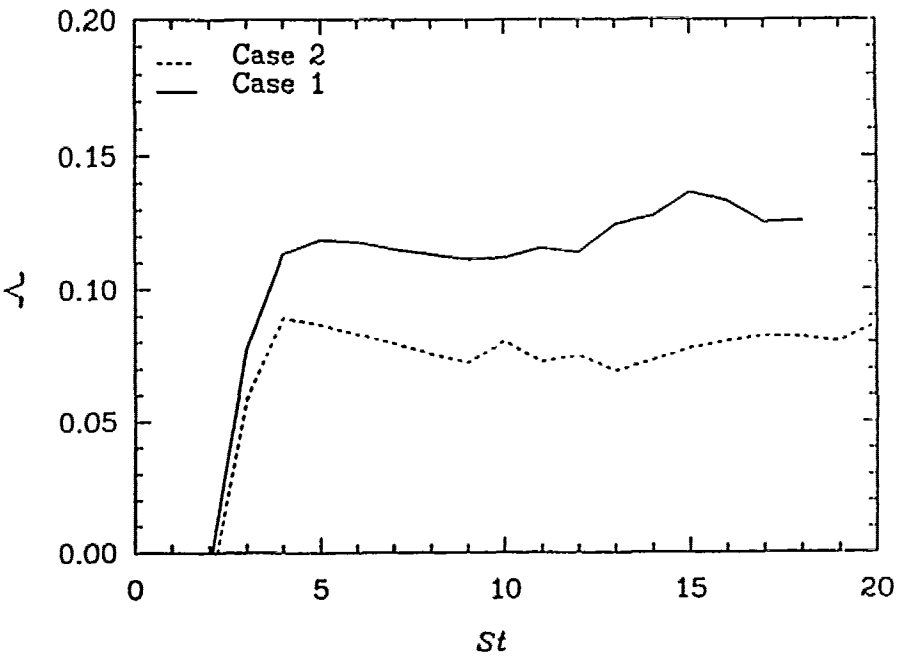

Fig. 3 Growth rate of turbulent kinetic energy.

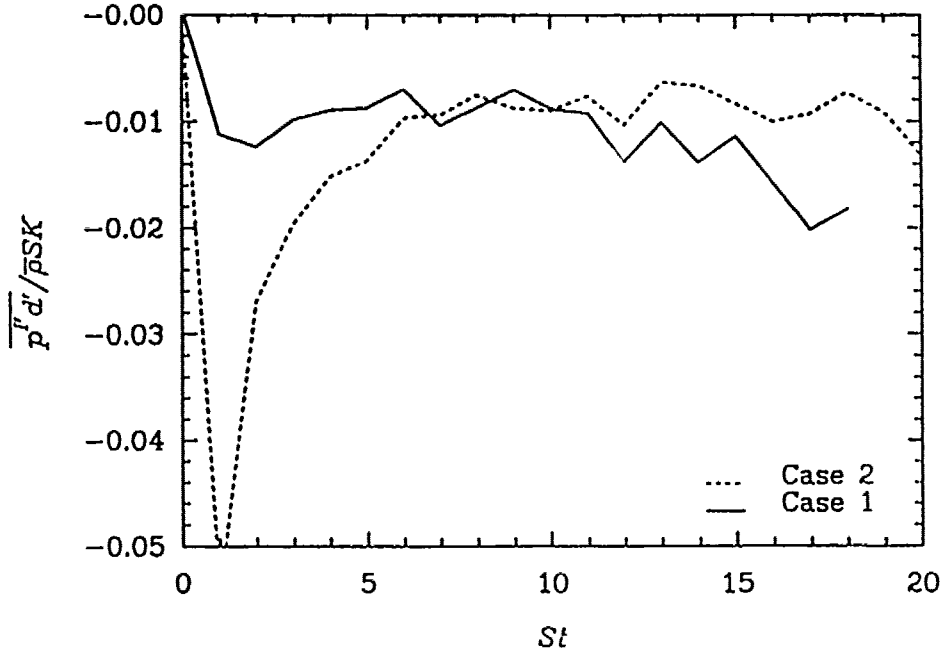

Fig. 4a. Contribution of pressure–dilatation to the growth rate of K.

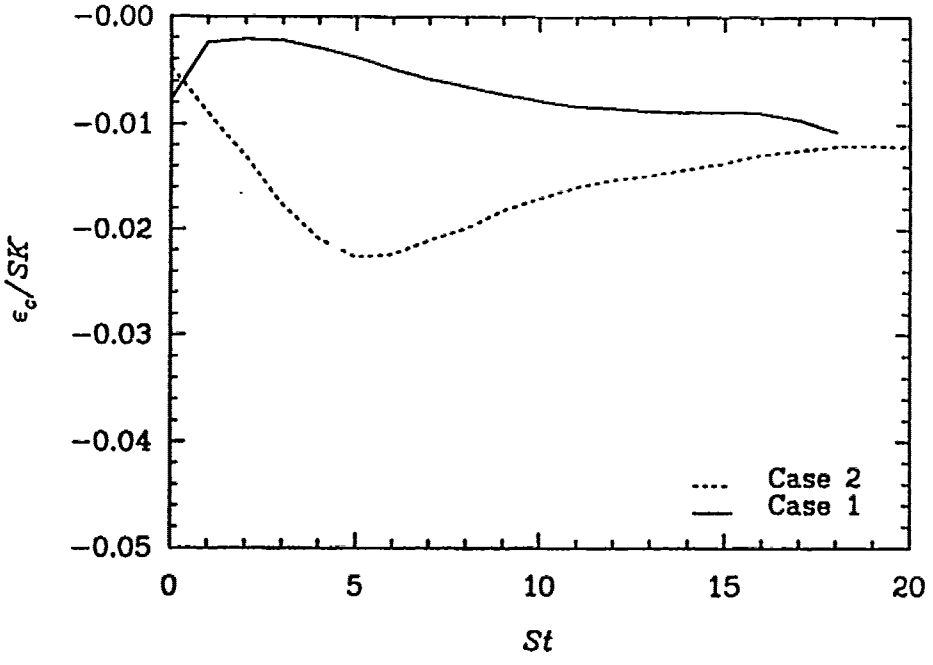

Fig. 4b. Contribution of compressible dissipation to the growth rate of K.

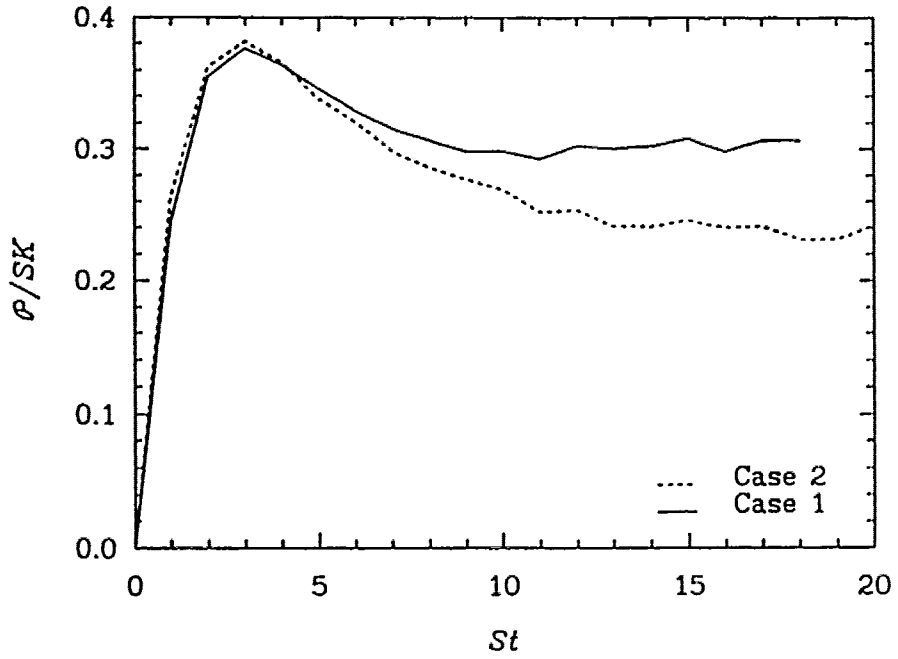

Fig. 4c. Contribution of production to the growth rate of K.

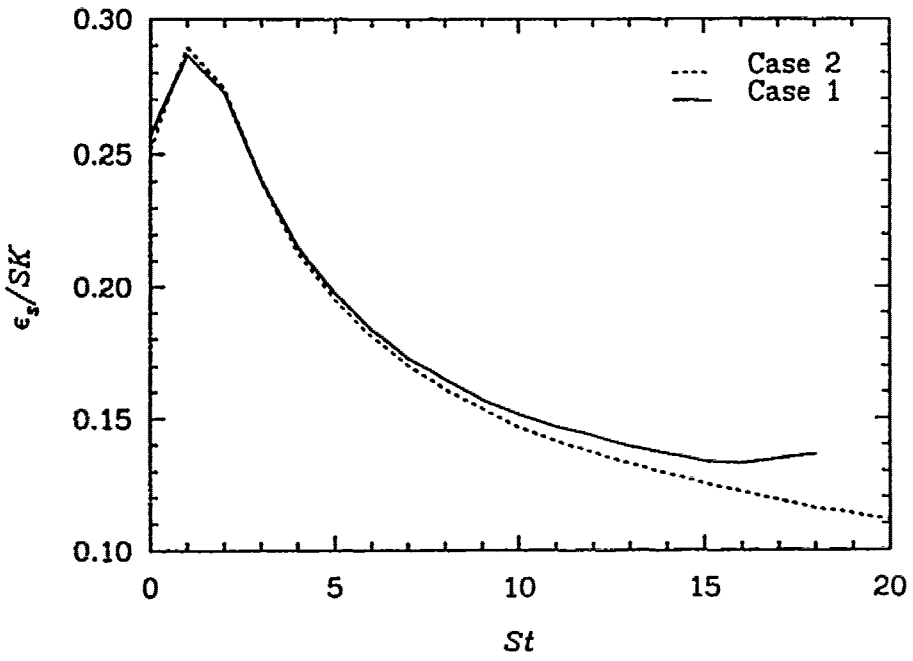

Fig. 4d. Contribution of solenoidal dissipation to the budget of K.

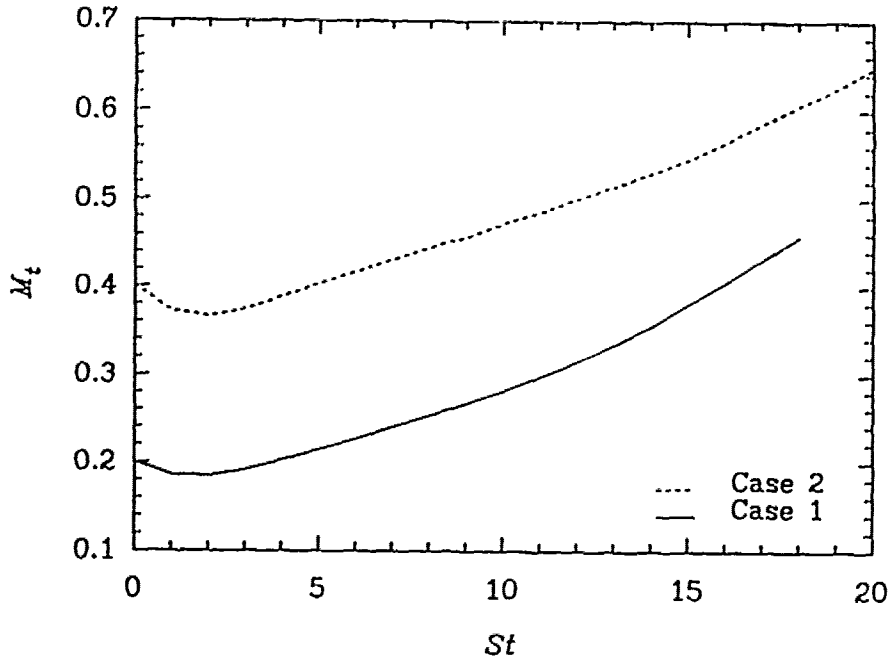

Fig. 5a. Evolution of turbulent Mach number.

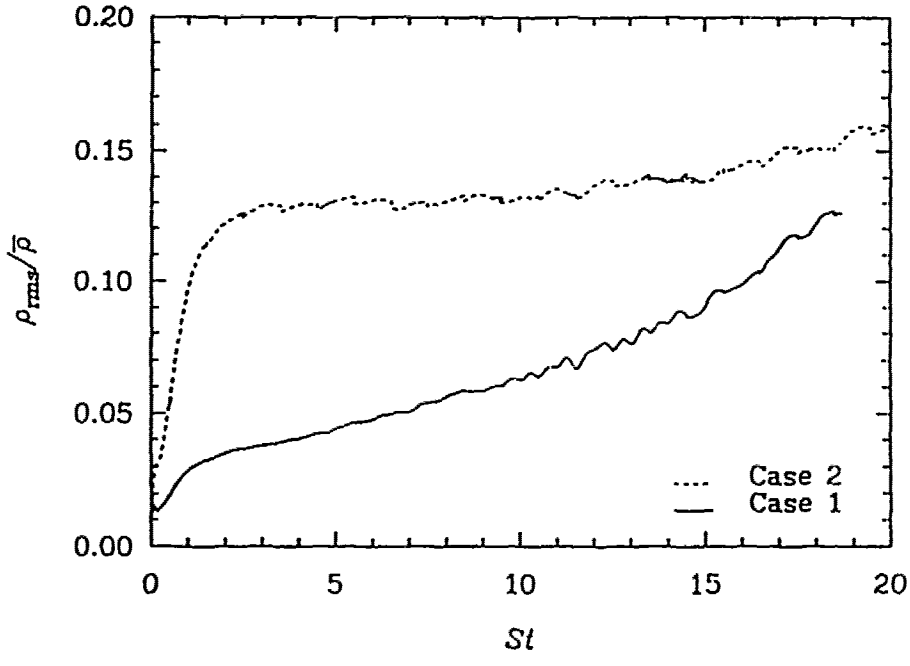

Fig. 5b. Evolution of rms density.

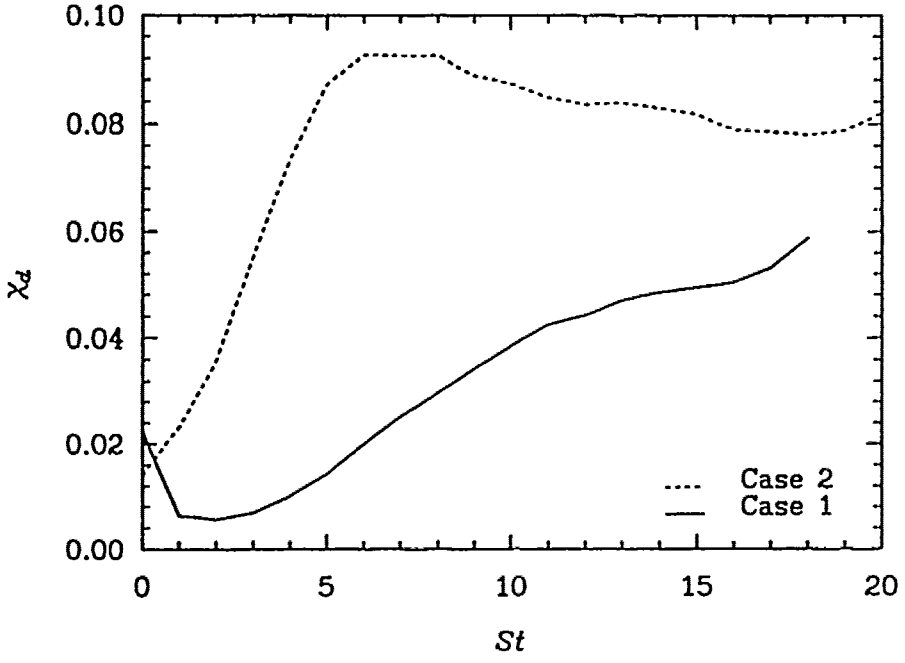

Fig. 6. Evolution of ratio of dilatational variance to enstrophy.

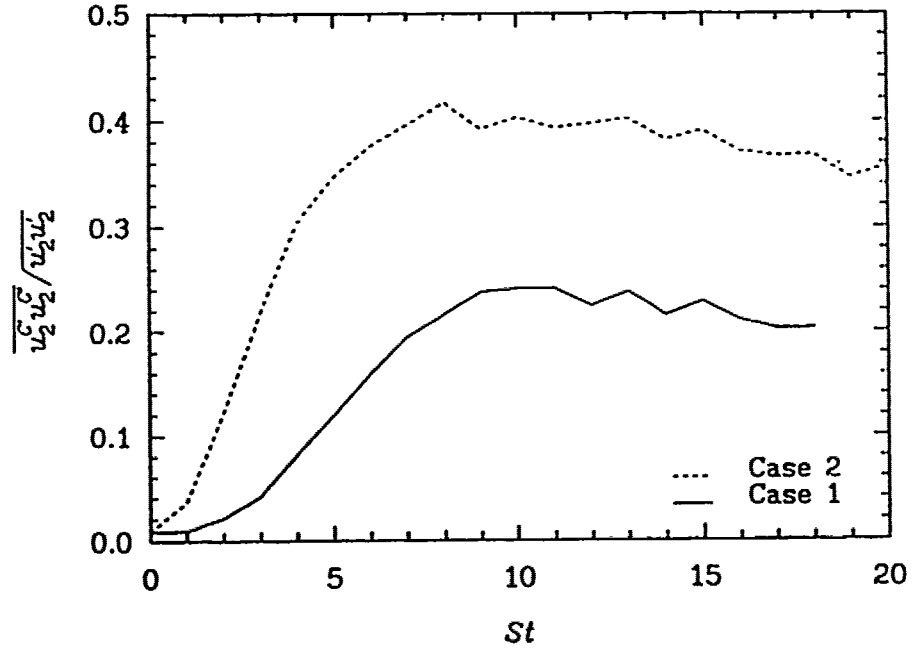

Fig. 7. Compressible fraction of transverse Reynolds stress.

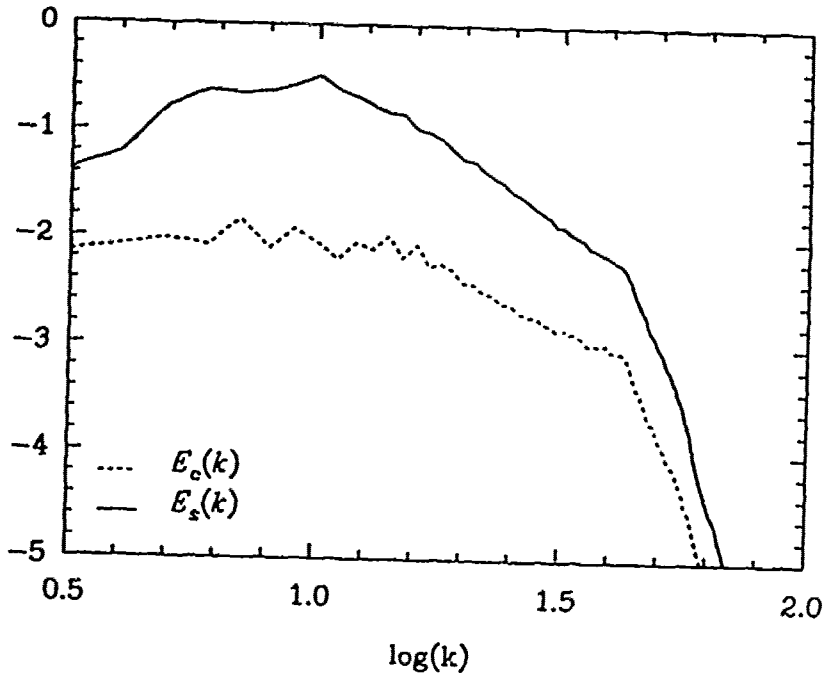

Fig. 8. Energy spectra at St=15 for Case 2.

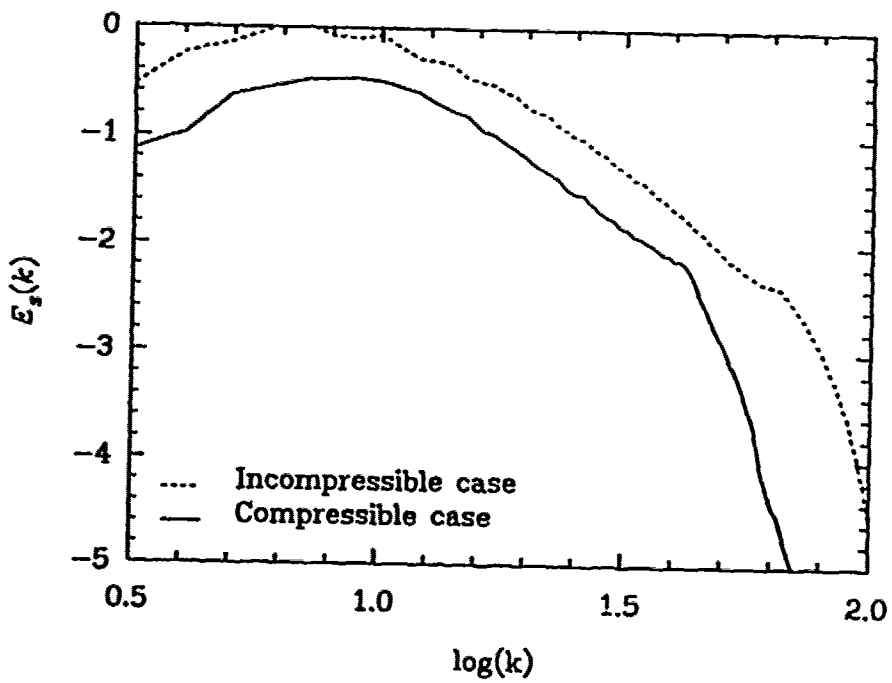

Fig. 9. Solenoidal velocity spectra for compressible and incompressible runs.

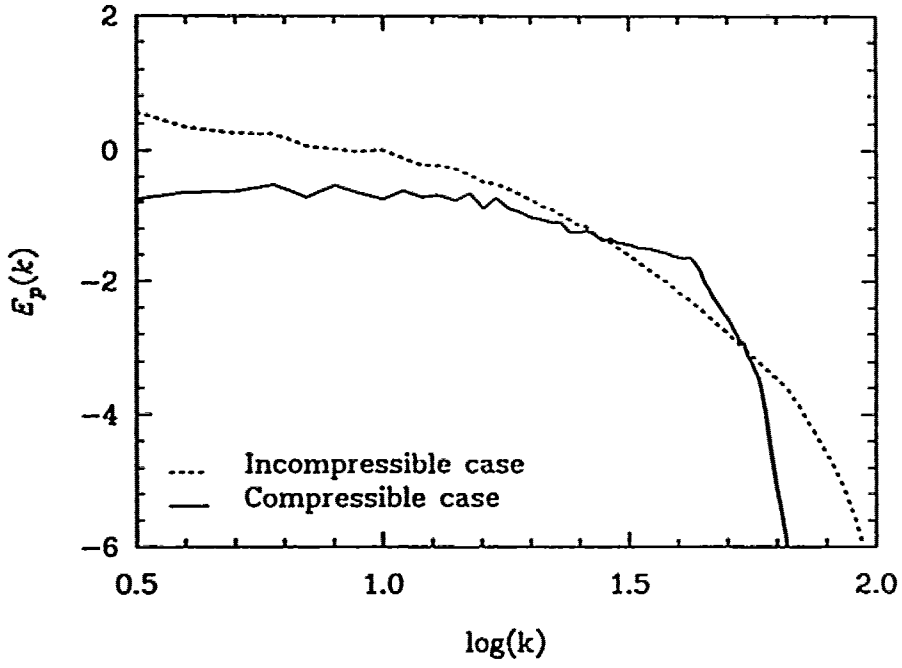

Fig. 10. Pressure spectra for compressible and incompressible runs.

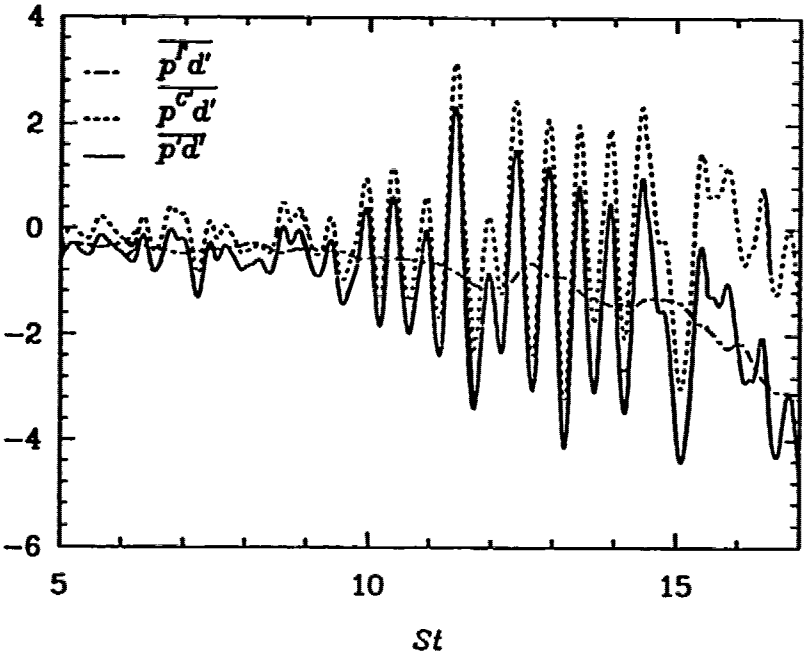

Fig. 11. Evolution of pressure–dilatation in Case 1.

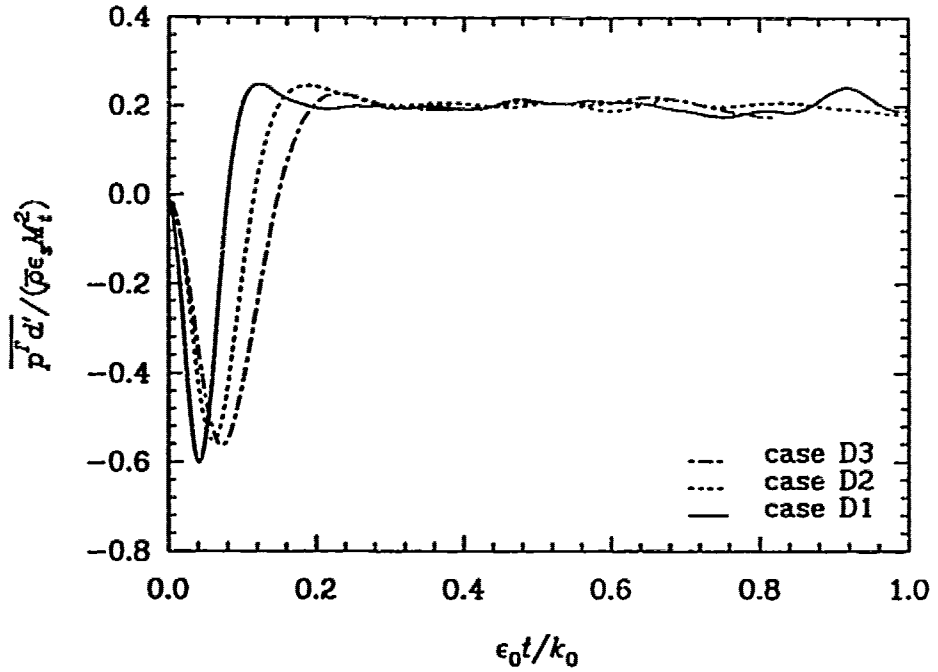

Fig. 12. Incompressible pressure–dilatation in decaying isotropic turbulence.

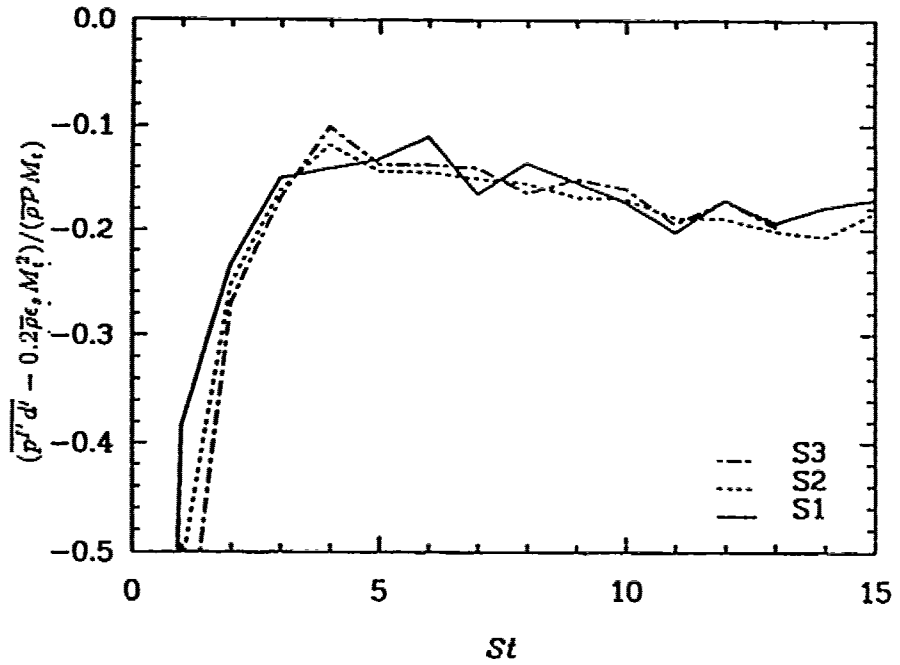

Fig. 13. Incompressible pressure–dilatation in homogeneous shear turbulence.

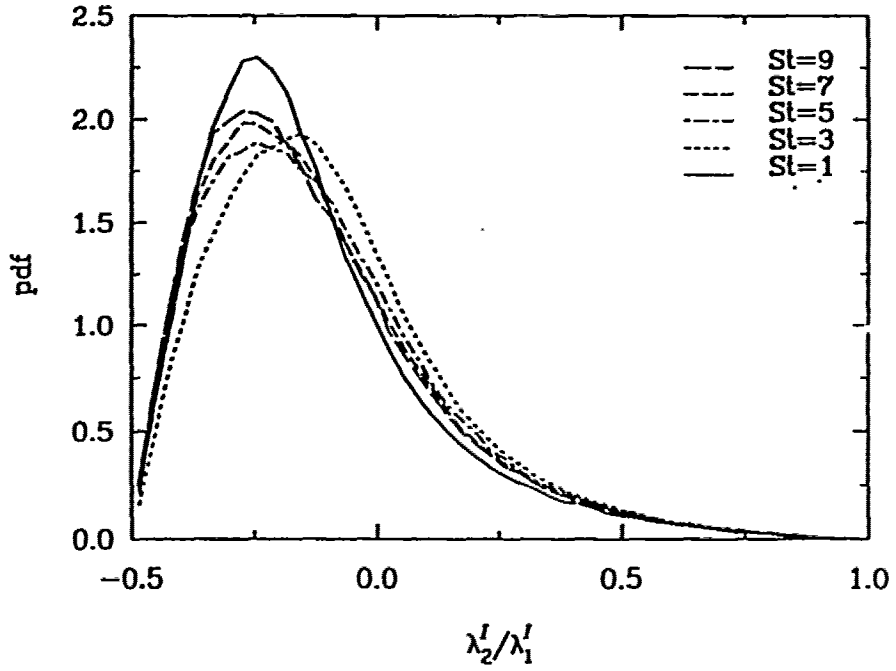

Fig. 14. Pdf of solenoidal eigenvalue ratio.

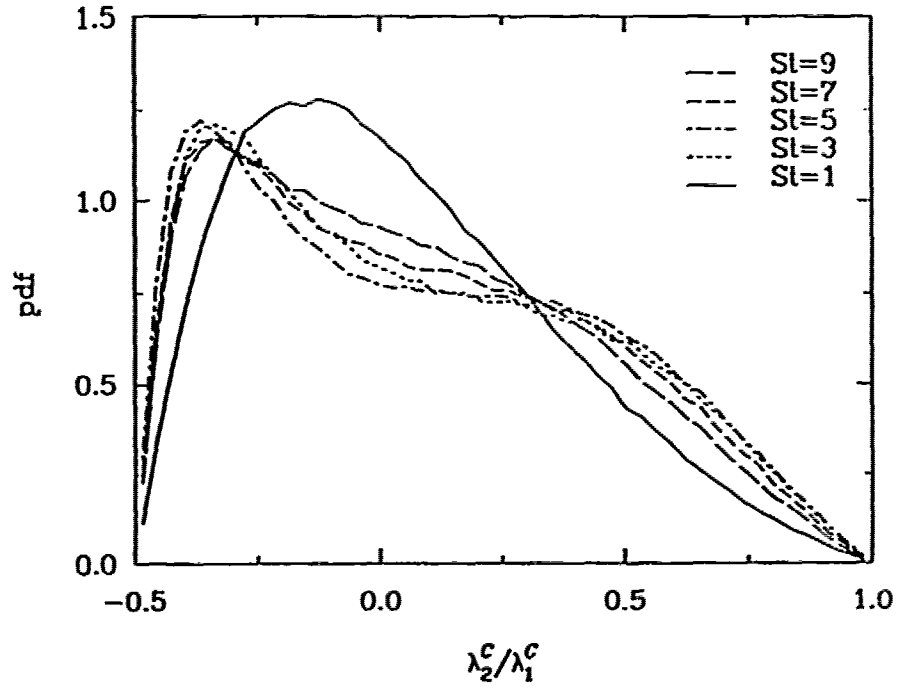

Fig. 15. Pdf of irrotational eigenvalue ratio.

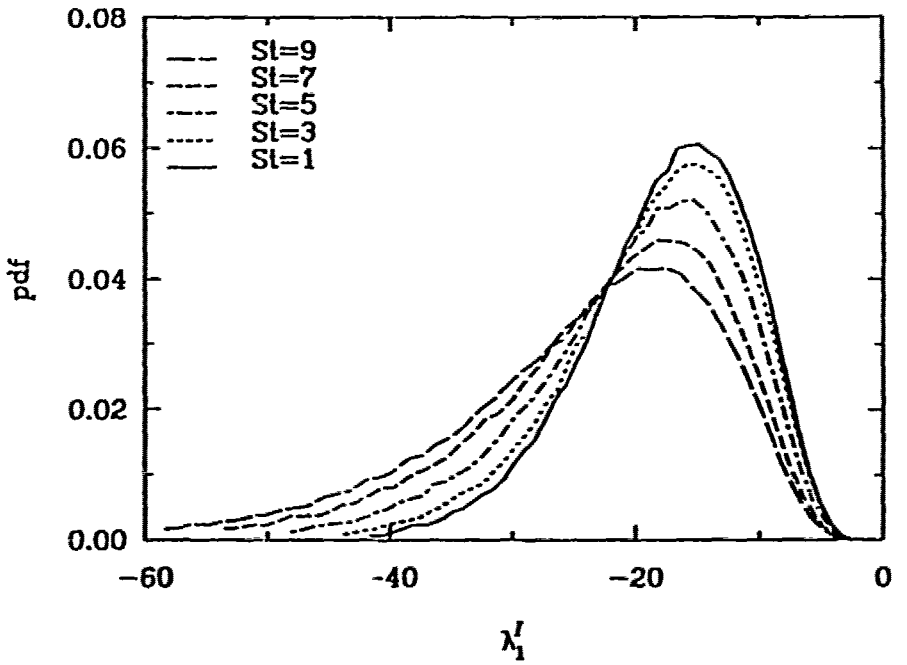

Fig. 16. Pdf of most compressive solenoidal eigenvalue.

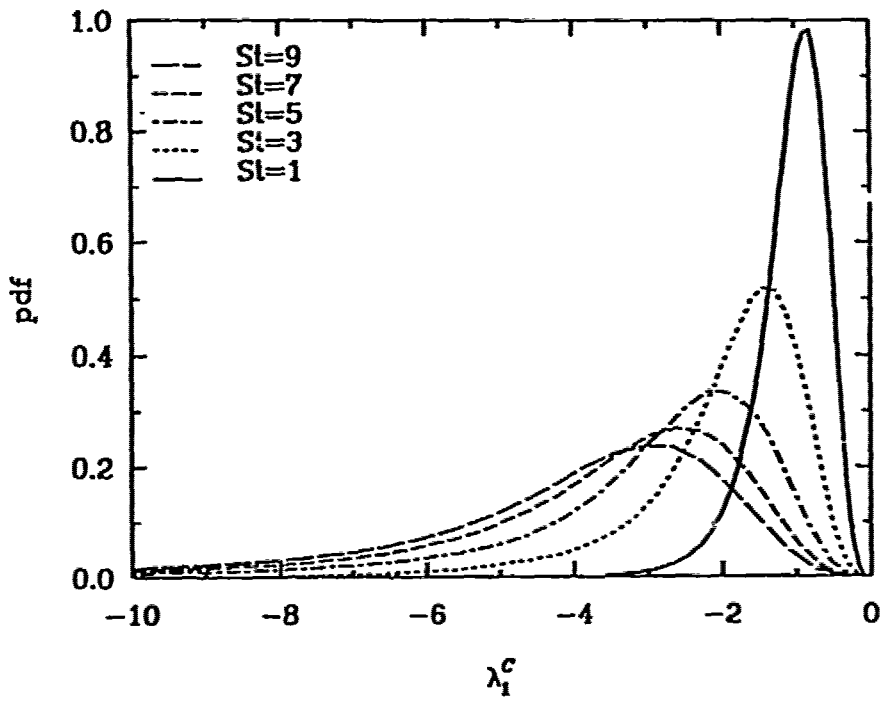

Fig. 17. Pdf of most compressive irrotational eigenvalue.

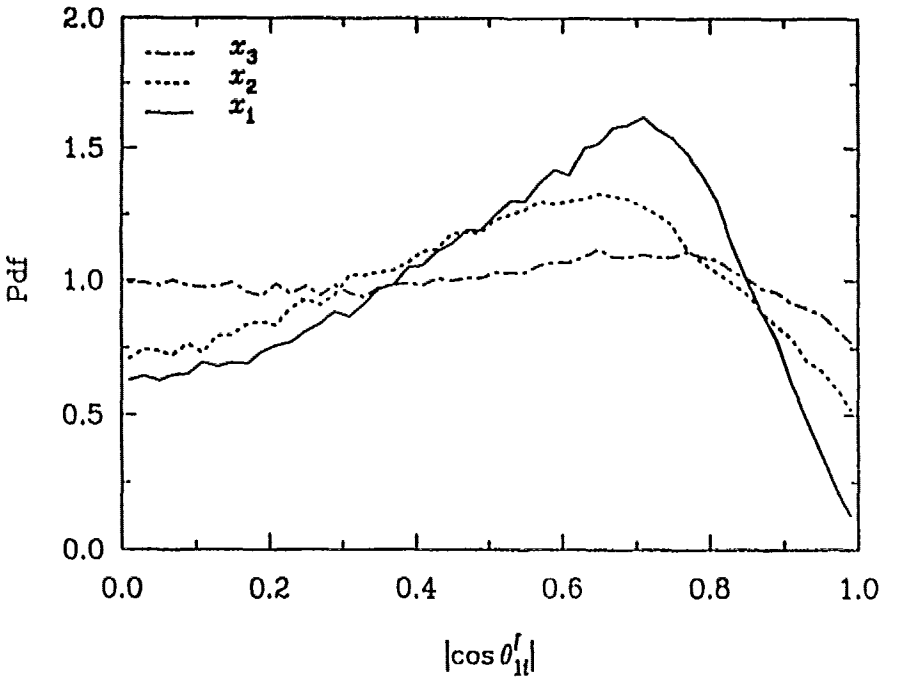

Fig. 18. Pdf of the orientation of the most compressive solenoidal eigenvector with respect to the three coordinate axes.

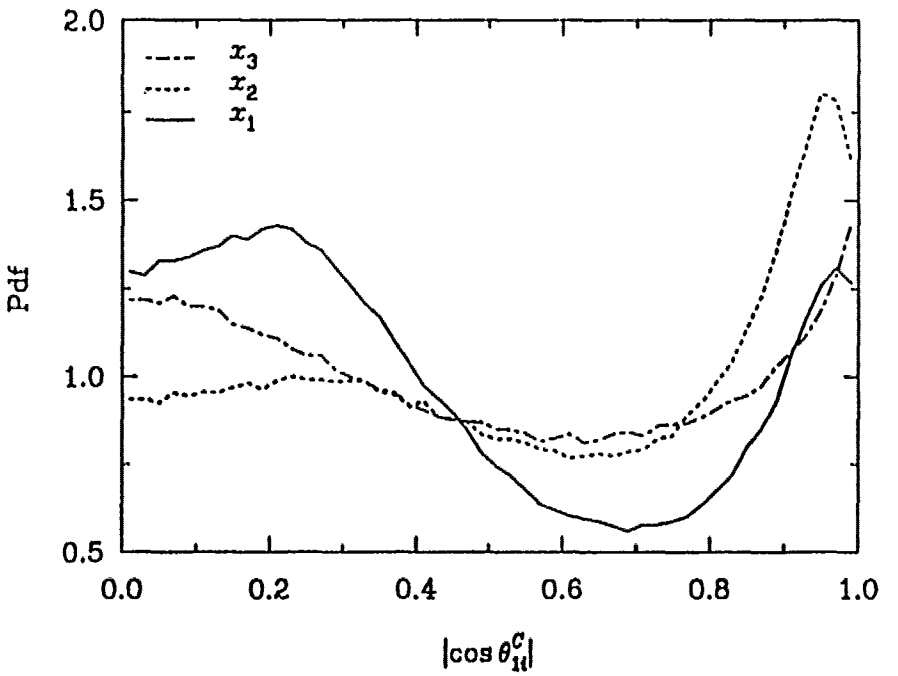

Fig. 19. Pdf of the orientation of the most compressive irrotational eigenvector with respect to the three coordinate axes.

REPORT DOCUMENTATION PAGE

Form Approved
OMB No 0704-0188

1. AGENCY USE ONLY (Leave blank)	2. REPORT DATE	3. REPORT TYPE AND DATES COVERED
	February 1992	Contractor Report

4. TITLE AND SUBTITLE
COMPRESSIBLE HOMOGENEOUS SHEAR: SIMULATION AND MODELING

5. FUNDING NUMBERS
C NAS1-18605
WU 505-90-52-01

6. AUTHOR(S)
S. Sarkar, G. Erlebacher, and M. Y. Hussaini

7. PERFORMING ORGANIZATION NAME(S) AND ADDRESS(ES)
Institute for Computer Applications in Science and Engineering
Mail Stop 132C, NASA Langley Research Center
Hampton, VA 23665-5225

8. PERFORMING ORGANIZATION REPORT NUMBER
ICASE Report No. 92-6

9. SPONSORING/MONITORING AGENCY NAME(S) AND ADDRESS(ES)
National Aeronautics and Space Administration
Langley Research Center
Hampton, VA 23665-5225

10. SPONSORING/MONITORING AGENCY REPORT NUMBER
NASA CR-189611
ICASE Report No. 92-6

11. SUPPLEMENTARY NOTES
Langley Technical Monitor: Michael F. Card
Final Report
To appear in 'Turbulent Shear Flows 8: Selected Papers' (1992)

12a. DISTRIBUTION/AVAILABILITY STATEMENT
Unclassified - Unlimited

Subject Category 34

12b. DISTRIBUTION CODE

13. ABSTRACT *(Maximum 200 words)*

The present study investigates compressibility effects on turbulence by direct numerical simulation of homogeneous shear flow. A primary observation is that the growth of the turbulent kinetic energy decreases with increasing turbulent Mach number. The sinks provided by compressible dissipation and the pressure-dilatation, along with reduced Reynolds shear stress, are shown to contribute to the reduced growth of kinetic energy. Models are proposed for these dilatational terms and verified by direct comparison with the simulations. The differences between the incompressible and compressible fields are brought out by the examination of spectra, statistical moments, and structure of the rate of strain tensor.

14. SUBJECT TERMS
compressible flow, turbulence

15. NUMBER OF PAGES
27

16. PRICE CODE
A03

17. SECURITY CLASSIFICATION OF REPORT	18. SECURITY CLASSIFICATION OF THIS PAGE	19. SECURITY CLASSIFICATION OF ABSTRACT	20. LIMITATION OF ABSTRACT
Unclassified	Unclassified		